

# The Size Distribution of Superbubbles in the Interstellar Medium

By M. S. OEY AND C. J. CLARKE

Institute of Astronomy, Madingley Road, Cambridge, CB3 0HA, UK

We use the standard, adiabatic shell evolution to predict the size distribution  $N(R)$  for populations of SN-driven superbubbles in a uniform ISM. We derive  $N(R)$  for simple cases of superbubble creation rate and mechanical luminosity function. We then compare our predictions for  $N(R)$  with the largely complete H I hole catalogue for the SMC, with a view toward the global structure of the ISM in that galaxy. We also present a preliminary derivation for  $N(v)$ , the distribution of shell expansion velocities.

---

## 1. Introduction

Core-collapse supernovae (SNe) tend to be correlated in both space and time because of the clustering of the massive ( $\gtrsim 8 M_{\odot}$ ) star progenitors. These clustered SNe, along with stellar winds of the most massive stars, produce superbubble structures in both the warm ionized ( $10^4$  K) and atomic H I components of the interstellar medium (ISM) in star-forming galaxies. The hot, coronal component of the ISM is thought to originate largely from the shock heating of material interior to shells of superbubbles and supernova remnants (SNRs). Total kinetic energies deposited into the interstellar environment are in the range  $10^{51} - 10^{54}$  erg for OB associations, and  $\gtrsim 10^{55}$  erg for starburst phenomena. Hence, the large-scale structure and kinematics of the multi-phase ISM could be largely determined by this superbubble activity. Likewise, this effect should influence turbulence on global, macroscopic scales, which then cascades to smaller scales.

The standard model for understanding superbubble evolution is the adiabatic model for a continuous mechanical energy input (Pikel'ner 1968; Weaver *et al.* 1977; Dyson 1977), where the sequential SNe from the parent star cluster are treated as a continuous power source (McCray & Kafatos 1987). The evolution of the shell parameters can then be described by a set of simple, self-similar relations analogous to the Sedov (1959) model for a single point energy injection. How applicable is the standard, adiabatic model to the long-term evolution of superbubbles? It is possible to make some rudimentary assumptions about the global ambient ISM and shell creation history, and then use the analytic equations to derive a superbubble size distribution that is predicted by the model. Such a size distribution can then be compared to observed H I shell catalogues to gain insight into the global structure and kinematics of the ISM. Variations from the prediction can then point to important effects that have not been adequately treated.

In this contribution, we summarize our derivation of the superbubble size distribution, which is described in greater detail by Oey & Clarke (1997). We compare our results to the H I shell catalogue of the Small Magellanic Cloud (SMC). Finally, we present preliminary new results for an analogous derivation of the distribution of shell expansion velocities.

## 2. Assumptions

Our purpose is to make the simplest feasible assumptions to see what the standard shell evolution predicts in the simplest conditions. Our assumptions are thus as follows.

We assume coeval star formation in the parent clusters, which produce a constant

mechanical power  $L$  until the lowest-mass SN progenitors expire at an age  $t_e = 40$  Myr. Studies of OB associations in the Magellanic Clouds and the Galaxy (Massey *et al.* 1995a, b) show stellar age spreads of  $\lesssim 3$  Myr, motivating our adoption of coeval star formation. Likewise, stellar population synthesis modeling by Shull & Saken (1995) and Leitherer & Heckman (1995) suggests that the assumption of constant  $L$  appears to be reasonable. We also assume that the stellar initial mass function (IMF) remains fixed and universal, and we adopt a uniform and infinite ambient ISM.

Based on the observed power-law form of the H II region luminosity function (H II LF; e.g. Kennicutt *et al.* 1989), we infer a similar power-law distribution of parent cluster masses. For a constant IMF, the nebular H $\alpha$  luminosity scales directly with the number of stars, and likewise,  $L$  for the clusters is directly proportional to the number of core-collapse SN progenitors. We therefore take the mechanical luminosity function (MLF) for the cluster population to be a power-law as well:

$$\phi(L) = \frac{dN}{dL} = AL^{-\beta} \quad , \quad (2.1)$$

normalized such that  $\int \phi(L) dL = 1$ . Ordinarily, the power-law index  $\beta$  of the MLF should be identical to that of the associated H II LF. We caution that evolutionary effects and small-number statistics in the stellar population can complicate this assumption (Oey & Clarke 1997, 1998), but essentially the power-laws are the same. We also consider one scenario with a single-valued MLF. In conjunction with these forms of the MLF, we consider a constant shell creation rate  $\psi$ , and a single-burst creation model.

The treatment of the endstage evolution for the superbubbles is crucial, but extremely uncertain. We assume that the shell growth stalls at an age  $t_f$  when the superbubble's internal pressure  $P_i \leq P_0$ , the ambient ISM pressure. Such a scenario is supported by numerical simulations (García-Segura & Franco 1996), in which radiative energy loss at this endstage suppresses further growth of the superbubble cavity. We then assume that the shell maintains this stall radius  $R_f$  until the input power stops at time  $t_e$ . However, objects that never achieve pressure equilibrium with the ambient ISM continue to grow until  $t_e$ . The subsequent destruction of the shells is even more uncertain. We simply assume that all objects survive for a nominal, universal period  $t_s \ll t_e$  and vanish thereafter. We note that if the breakup of shells into smaller holes occurs such that the ratio of subunit sizes is universal for all objects, then an original power-law size distribution remains unaffected (Clarke 1996).

### 3. Analytic Prediction

The standard evolution predicts that the shell radius grows as (e.g. Weaver *et al.* 1977):

$$R = \left( \frac{250}{308\pi} \right)^{1/5} L^{1/5} \rho^{-1/5} t^{3/5} \quad , \quad (3.2)$$

where  $t$  is elapsed time,  $\rho$  is the mass density of a uniform ambient medium, and all units are cgs. The pressure interior to the shell will decline as:

$$P_i = \frac{7}{(3850\pi)^{2/5}} L^{2/5} \rho^{3/5} t^{-4/5} \quad . \quad (3.3)$$

From equations 3.2 and 3.3 we see that the stall criterion  $P_i = P_0$  yields a correspondence between stall age and radius, uniquely determined by the input  $L$ . The characteristic time scale  $t_e$  therefore determines the associated parameters  $R_e$  and  $L_e$ ; hence, a superbubble with input power  $L_e$  will stall at exactly age  $t_e$  with radius  $R_e$ . It is thus apparent that objects with input power  $L < L_e$  will follow an evolution that stalls at

some point before  $t_e$ , and remain at radii  $R < R_e$ ; whereas those with  $L > L_e$  will never stall, and at some point before  $t_e$  will grow to radii  $R > R_e$ . For an ambient number density  $n = 0.5 \text{ cm}^{-3}$ , mean particle weight  $\mu = 1.25$ , and  $P_0 = 3 \times 10^{-12} \text{ dyne cm}^{-2}$ , the adopted  $t_e = 40 \text{ Myr}$  implies  $R_e = 1300 \text{ pc}$  and  $L_e = 2.2 \times 10^{39} \text{ erg s}^{-1}$ .

These characteristic parameters are useful as scaling parameters, hence we have,

$$\frac{R}{R_e} = \left(\frac{L}{L_e}\right)^{1/5} \left(\frac{t}{t_e}\right)^{3/5}, \quad (3.4)$$

$$\frac{P_i}{P_0} = \left(\frac{L}{L_e}\right)^{2/5} \left(\frac{t}{t_e}\right)^{-4/5}, \quad (3.5)$$

and

$$\frac{t_f}{t_e} = \frac{R_f}{R_e} = \left(\frac{L}{L_e}\right)^{1/2}. \quad (3.6)$$

We now derive the differential superbubble size distribution  $N(R)$  for specific combinations of shell creation history and MLF. We define  $N(R) dR$  as the number of objects with radii in the range  $R$  to  $R + dR$ .

### 3.1. Continuous Creation, Single Luminosity

For a continuous and constant superbubble creation rate  $\psi$  and a single-valued MLF with  $\phi(L) = L_0$ , the size distribution for growing shells is given by,

$$N_{\text{grow}}(R) = \psi \left(\frac{\partial R}{\partial t}\right)^{-1}. \quad (3.7)$$

The size distribution for the stalled objects is clearly a  $\delta$ -function at the stall radius associated with  $L_0$ , whose magnitude is determined by the length of the creation period:

$$N_{\text{stall}}(R) = \psi \left(t_e - t_f(L_0)\right) \cdot \delta\left(R - R_f(L_0)\right), \quad (3.8)$$

where  $t_f(L_0)$  and  $R_f(L_0)$  are the stall parameters for a shell powered by  $L_0$ . The distribution in  $R$  is therefore determined exclusively by the growing objects. Applying the relations for the standard evolution given above, equation 3.7 gives,

$$N_{\text{grow}}(R) = \frac{5}{3} \psi \frac{t_e}{R_e} \left(\frac{L_0}{L_e}\right)^{-1/3} \left(\frac{R}{R_e}\right)^{2/3}. \quad (3.9)$$

We define the power-law slope of the size distribution as  $\alpha$ , analogously to that of the MLF (equation 2.1), such that  $N(R) \propto R^{-\alpha}$ . The case here is the only one for which we derive a positive power-law index in  $R$ , yielding  $-\alpha = \frac{2}{3}$ . The positive index is induced by the single-valued MLF.

### 3.2. Single Burst Creation, Luminosity Spectrum

We now consider the inverse case of instantaneous creation of all the objects, with a power-law MLF given by equation 2.1. Here, the size distributions for the growing and stalled objects are given by,

$$N_{\text{grow}}(R) = N_b \phi(L) \left(\frac{\partial R}{\partial L}\right)^{-1} \quad (3.10)$$

and

$$N_{\text{stall}}(R) = N_b \phi(L) \left(\frac{\partial R_f}{\partial L}\right)^{-1}, \quad (3.11)$$

respectively, where  $N_b$  is the number of objects created in the burst. Applying the standard evolution, we obtain,

$$N_{\text{grow}}(R) = 5AN_b(1 - F_{\text{st}}) \frac{L_e^{1-\beta}}{R_e} \left(\frac{R}{R_e}\right)^{4-5\beta} \left(\frac{t}{t_e}\right)^{-3+3\beta} \quad (3.12)$$

and

$$N_{\text{stall}}(R) = 2AN_b F_{\text{st}} \frac{L_e^{1-\beta}}{R_e} \left(\frac{R}{R_e}\right)^{1-2\beta}, \quad (3.13)$$

where  $F_{\text{st}}$  is the fraction of stalled shells:

$$F_{\text{st}} = \int_{L_{\text{min}}}^{L_{\text{st}}(t)} AL^{-\beta} dL, \quad (3.14)$$

where  $L_{\text{st}}(t)$  is the luminosity corresponding to  $t = t_f$ , i.e., the largest stalled shells. The lower limit of integration,  $L_{\text{min}}$ , is the lower- $L$  cutoff in the MLF, which in our analysis corresponds to the mechanical power associated with individual SNe.

The H II LF in nearby galaxies typically has a power-law index of  $2.0 \pm 0.3$  (e.g. Kennicutt *et al.* 1989), implying that value for  $\beta$ . Hence, the power-law exponents of  $N(R)$  given by equations 3.12 and 3.13 are negative, and we have  $\alpha \simeq 6$  and 3, for growing and stalled objects, respectively.

We find that the stalled superbubbles generally dominate the total  $N(R)$ , owing to the large numbers of weak- $L$  objects. Therefore, the observed shell size distribution should be described essentially by equation 3.13, having a slope  $-\alpha = 1 - 2\beta$ . However, this will extend only to the stall radius associated with the age of the burst  $t_b$ , since higher- $L$  objects will not have had enough time to stall. Objects with  $R > R_f(t_b)$  must therefore be growing shells, described by equation 3.12, having a much steeper dropoff with  $-\alpha = 4 - 5\beta$ . There is a discontinuous jump in  $N(R)$  by a factor of  $\frac{5}{2}$  at  $R_f(t_b)$ .

We therefore suggest that the existence, and age, of a recent single burst event can be discerned from the shell size distribution.

### 3.3. Continuous Creation, Luminosity Spectrum

In the most general case, continuous creation with a power-law MLF, the two different shell evolutions for  $L < L_e$  and  $L > L_e$  yield derivations for  $N(R)$  that produce different solutions for the regimes  $R < R_e$  and  $R > R_e$ . Since  $R_e$  is very large ( $\gtrsim 1$  kpc), we are primarily interested in the regime for  $R < R_e$ .

For this case, superbubbles in the growing phase are described by,

$$N_{\text{grow}}(R) = \int_{t(R, L_{\text{max}})}^{t_f(R)} \psi \phi(L) \left(\frac{\partial R}{\partial L}\right)^{-1} dt. \quad (3.15)$$

The lower limit of integration corresponds to the youngest objects having radius  $R$ , which are set by an upper- $L$  limit  $L_{\text{max}}$ . The upper limit of integration is the stall age corresponding to  $R$  (equation 3.6). For the standard evolution, equation 3.15 yields,

$$N_{\text{grow}}(R) = 5A\psi \frac{L_e^{1-\beta}}{R_e} \frac{t_e}{-2 + 3\beta} \left(\frac{R}{R_e}\right)^{2-2\beta}. \quad (3.16)$$

Similarly, stalled objects are given by,

$$N_{\text{stall}}(R) = \int_{t_f(R)}^{t_e} \psi \phi(L) \left(\frac{\partial R_f}{\partial L}\right)^{-1} dt. \quad (3.17)$$

Applying the standard evolution:

$$N_{\text{stall}}(R) = 2A\psi \frac{L_e^{1-\beta}}{R_e} t_e \left(\frac{R}{R_e}\right)^{1-2\beta} \left(1 - \frac{R}{R_e}\right) . \quad (3.18)$$

Finally, objects surviving for a period  $t_s$ , beyond  $t_e$ , are described by,

$$N_{\text{sur}}(R) = \int_{t_e}^{t_e+t_s} \psi dt \phi(L) \left(\frac{\partial R_f}{\partial L}\right)^{-1} , \quad (3.19)$$

yielding,

$$N_{\text{sur}}(R) = 2A\psi \frac{L_e^{1-\beta}}{R_e} t_s \left(\frac{R}{R_e}\right)^{1-2\beta} . \quad (3.20)$$

Adding together equations 3.16, 3.18, and 3.20 for the populations in the three evolutionary stages, we obtain an overall size distribution (for  $\beta > \frac{2}{3}$ ):

$$N(R) = A\psi \frac{L_e^{1-\beta}}{R_e} \left(\frac{R}{R_e}\right)^{1-2\beta} \left[ 2(t_e + t_s) + \frac{9 - 6\beta}{-2 + 3\beta} t_e \left(\frac{R}{R_e}\right) \right] . \quad (3.21)$$

Equation 3.21 has two terms in  $R$ . As in the single-burst case, the stalled shells with the dependence  $-\alpha = 1 - 2\beta$  dominate  $N(R)$ . An observed shell size distribution would therefore resemble this power-law in the range  $R_f(L_{\min}) < R < R_e$ . The lower limit represents the smallest stalled shells, which, in our treatment, correspond to individual SNRs. We caution that the assumption of constant  $L$  breaks down in this regime, since individual SNe are discrete events. However, the peak in  $N(R)$  should still be due to these single SNRs.

For  $R < R_f(L_{\min})$ , we recover growing objects, for which equation 3.15 is now dominated by the lower limit of integration, yielding:

$$N_{\text{grow}}(R) = 5A\psi \frac{L_e^{1-\beta}}{R_e} \left(\frac{L_{\max}}{L_e}\right)^{\frac{2}{3}-\beta} \frac{-t_e}{-2 + 3\beta} \left(\frac{R}{R_e}\right)^{2/3} . \quad (3.22)$$

Note that for this population, we again find the positive power-law slope  $-\alpha = \frac{2}{3}$ , that we obtained for a single-valued  $\phi(L)$  (equation 3.9). The case here is analogously dominated by the upper- $L$  limit,  $L_{\max}$ .

The size distribution in the regime  $R > R_e$  is derived from relations similar to equations 3.15, 3.17, and 3.19, with different limits of integration. We derive a final size distribution for these supergiant shells:

$$N(R) = 5A\psi \frac{L_e^{1-\beta}}{R_e} \left(\frac{R}{R_e}\right)^{4-5\beta} \left[ \frac{t_e}{-2 + 3\beta} + t_s \right] . \quad (3.23)$$

This population consists entirely of growing objects, along with a few shells in the survival stage. As seen in the case of the single burst, we again find a steep size distribution with  $-\alpha = 4 - 5\beta$ . Of course, given the numbers of objects, and breakdown of basic assumptions at these sizes, it is impracticable to compare the result to observations in this regime.

#### 4. Comparison with Observations

Now taking the observed slope of the H II LF to be the same as  $\beta$ , as argued in § 2, we can make a prediction for  $N(R)$  and compare with observed H I shell catalogues. Figure 1 shows the histogram for the size distribution of H I holes observed in the SMC (Staveley-Smith *et al.* 1997). We predict  $N(R)$  for this galaxy using the H II LF slope

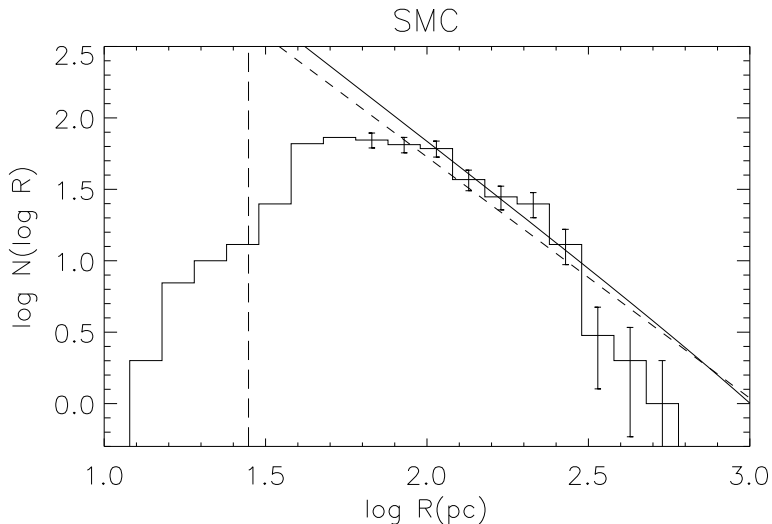


FIGURE 1. Histogram of catalogued H I shell radii in the SMC (Staveley-Smith *et al.* 1997). The observed power-law slope  $\alpha_o = 2.7 \pm 0.6$  was fitted from the bins with error bars (dashed line); the predicted slope  $\alpha_p = 2.8 \pm 0.4$  is shown by the solid line, normalized to the data at  $R = 100$  pc. The H I survey resolution limit is shown by the vertical long-dashed line. [Note that the slope of  $\log N(\log R)$  vs.  $\log R$  is  $1 - \alpha$ .]

measured by Kennicutt *et al.* (1989). We fitted a power-law slope to the H I data (dashed line) from the bins marked with error bars, yielding the observed slope  $\alpha_o = 2.7 \pm 0.6$ . The slope of our prediction (solid line)  $\alpha_p = 2.8 \pm 0.4$  is computed using  $\beta = 1.9 \pm 0.2$  from the H II LF, and is therefore completely independent from  $\alpha_o$ . We normalized the prediction to the observations at  $R = 100$  pc.

The shell catalogue for the SMC is by far the most complete available for any galaxy. We also examined M31, M33, and Holmberg II (see Oey & Clarke 1997), but the H I data for those galaxies is too incomplete to discuss in detail here. For the SMC, however, the ratio of H I holes with  $R > 100$  pc, to H II regions with H $\alpha$  luminosities  $> 10^{37}$  erg s $^{-1}$ , is consistent with the life expectancies of the holes and nebulae, assuming constant creation. We are therefore confident that the SMC shell catalogue is reasonably complete at those radii. Compilation of an updated version of the catalogue is in progress, in which the very largest radial bins are slightly augmented (Stanimirović *et al.* 1998). As seen in Figure 1, these new data may strengthen the derived power-law at large  $R$ .

The observations and prediction are in remarkably good agreement, considering the many simplistic assumptions made in § 2. We therefore suggest that the SN-driven superbubble activity is indeed the primary agent responsible for the SMC shells, and that *no other fundamental process is necessary to explain the H I superbubble structure in this galaxy*. It is interesting to note that the  $-\alpha = 1 - 2\beta$  power-law appears to be fairly robust, since it results from any evolution for which equation 3.6 applies. In particular, the rival momentum-conserving shell evolution also follows this relation, hence yielding the same power-law exponent for  $N_{\text{stall}}(R)$ .

It will be interesting to examine  $N(R)$  for more galaxies (e.g. Thilker 1998), and especially disks, where shell evolution should be affected by the non-uniform gas distribution. Surprisingly, the limited H I hole samples for M31 and especially, M33, do not exhibit evidence that a power-law  $N(R)$  is truncated by blowout effects (Oey & Clarke 1997).

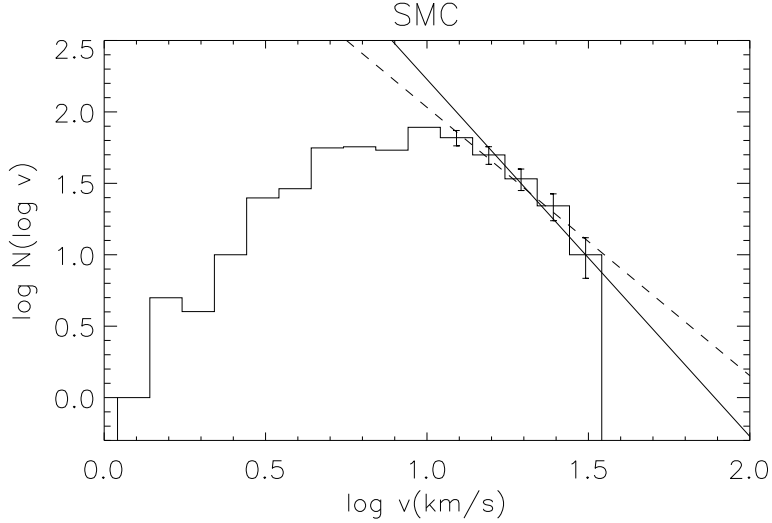


FIGURE 2. Histogram of shell expansion velocities for the SMC shell catalogue (Staveley-Smith *et al.* 1997). As in Figure 1, the power-law slope of  $-2.9 \pm 1.4$ , fit from the data, is shown by the dashed line. The solid line shows the predicted slope of  $-3.5$ , normalized to the data at the last bin.

## 5. Velocity Distribution

Here, we briefly present a preliminary derivation of  $N(v)$ , the distribution of superbubble expansion velocities. We will carry out a more complete study in a future paper. We consider the case of constant  $\psi$  and power-law  $\phi(L)$ , for the population of objects with  $R < R_e$ .  $N(v)$  is clearly determined only by the growing objects, hence by analogy to equation 3.15,

$$N_{\text{grow}}(v) = \int_{t(L_{\text{min}},v)}^{t(L_{\text{max}},v)} \psi \phi(L) \left( \frac{\partial v}{\partial L} \right)^{-1} dt \quad , \quad (5.24)$$

where

$$v = \frac{dR}{dt} = \frac{3 R_e}{5 t_e} \left( \frac{L}{L_e} \right)^{1/5} \left( \frac{t}{t_e} \right)^{-2/5} \quad . \quad (5.25)$$

The limits of integration in equation 5.24 are the ages corresponding to the least and most luminous objects yielding  $v$ . We obtain:

$$N(v) = -A\psi \frac{25}{3} \left( \frac{5}{3} \right)^{4-5\beta} \left( \frac{t_e}{R_e} \right)^{5-5\beta} \frac{t_e}{3-2\beta} L_e^{1-\beta} \left( \frac{L_{\text{min}}}{L_e} \right)^{3/2-\beta} v_c^{15/2-5\beta} v^{-7/2} \quad , \quad (5.26)$$

where  $v_c$  is the soundspeed of the ambient ISM. This velocity distribution applies to objects that have not stalled, namely, those with  $v \gtrsim v_c$ . Thus, we find a power-law dependence of  $v^{-7/2}$ , independent of  $\beta$ , although equation 5.26 is valid provided  $\beta > \frac{3}{2}$ .

In Figure 2 we show the histogram of expansion velocities for the SMC H I shell catalogue (Staveley-Smith *et al.* 1997). The fitted power-law slope is  $-2.9 \pm 1.4$ , which is in agreement within the large error. The large uncertainty is caused primarily by the short dynamic range in  $\log v$ , but Figure 2 shows that the power-law appears encouragingly well-behaved in comparison with the predicted slope.

## 6. Conclusion

We have presented analytic derivations of characteristics of the superbubble population under various simple conditions, as predicted by the standard, adiabatic shell evolution. This approach is useful in determining the roles of various phenomena in the global structure of the ISM and evolution of superbubbles. The preliminary agreement found between our prediction and H I observations for the size and velocity distributions of shells in the SMC suggests that SN-driven superbubble activity is likely to be the dominant source of structure in the neutral ISM of this, and other, galaxies. The velocity structure and turbulence in the ISM are also likely to be substantially determined by this activity.

Our analysis also yields other useful features that are discussed at greater length by Oey & Clarke (1997). For example, we predict a peak in  $N(R)$  at the stall radius of individual SNRs. Observations of  $N(R)$  might therefore provide an estimate for this radius, which could then be exploited to probe ISM densities, SN energies, and/or SNR evolution. The contribution of Type Ia SNRs should also be evident in  $N(R)$ . Our analysis is also readily applicable to the porosity of the ISM, which determines the relative importance, by volume, of the hot, coronal gas compared to the cooler phases of the ISM. Our study derives analytic expressions for both 2D and 3D porosity parameters. For three of the four galaxies examined, we found porosity parameters  $\lesssim 0.3$ , suggesting a fairly low filling factor for the hot ISM, although we caution that these values are sensitive to assumptions for the ambient interstellar conditions. We also applied this porosity analysis to the Galaxy, with inconclusive results.

We are grateful for discussions with E. Blackman, D. Cox, L. Drissen, J. Franco, D. Hatzidimitriou, C. Leitherer, C. Robert, J. Scalo, J.M. Shull, L. Staveley-Smith, and G. Tenorio-Tagle.

## REFERENCES

- CLARKE, C. J. 1996, *MNRAS* **283**, 353.  
 DYSON, J. E. 1977, *AA* **59**, 161.  
 GARCÍA-SEGURA G. & FRANCO J. 1996, *ApJ* **469**, 171.  
 KENNICUTT, R. C., EDGAR, B. K., HODGE, P. W. 1989, *ApJ* **337**, 761.  
 LEITHERER, C., HECKMAN, T. M. 1995, *ApJS* **96**, 9.  
 MASSEY, P., JOHNSON, K. E., & DEGIOIA-EASTWOOD, K., 1995, *ApJ* **454**, 151.  
 MASSEY, P., LANG, C. C., DEGIOIA-EASTWOOD, K., & GARMANY, C. D. 1995, *ApJ* **438**, 188.  
 MCCRAY, R. & KAFATOS, M. 1987, *ApJ* **317**, 190.  
 OEY, M. S. & CLARKE, C. J. 1997, *MNRAS* **289**, 570.  
 OEY, M. S. & CLARKE, C. J. 1998, *AJ*, in press.  
 PIKEL'NER, S. B. 1968, *Astrophys. Lett.* **2**, 97.  
 SEDOV, L. I. 1959, *Similarity and Dimensional Methods in Mechanics*, Academic, New York.  
 SHULL, J. M., SAKEN, J. M. 1995, *ApJ* **444**, 663.  
 STANIMIROVIĆ, S., STAVELEY-SMITH, L., DICKEY, J. M., SAULT, R. J., & SNOWDEN, S. L. 1998, *MNRAS*, in preparation.  
 STAVELEY-SMITH, L., SAULT, R. J., HATZIDIMITRIOU, D., KESTEVEN, M. J., MCCONNELL, D. 1997, *MNRAS* **289**, 225.  
 THILKER, D., this volume.  
 WEAVER, R., MCCRAY, R., CASTOR, J., SHAPIRO, P., & MOORE, R. 1977, *ApJ* **218**, 377.